



RESEARCH ARTICLE

Highly Deformable Microfluidic Sweat Sensors Fabricated via Roll-to-Roll Scalable Processes

Seung-Rok Kim^{1,2,3}  | Noelle Davis^{1,2,3} | Nicole Qing¹ | Liam Gillan⁵ | Elina Hakola⁶ | Olli-Heikki Huttunen⁵ | Johanna Hiitola-Keinänen⁶ | Youngho Song^{1,7} | Yullim Lee^{1,7} | Soo-Yeon Cho⁷ | Jussi Hiltunen⁶ | Ali Javey^{1,2,3,4} 

¹Department of Electrical Engineering and Computer Sciences, University of California Berkeley, California, USA | ²Materials Sciences Division, Lawrence Berkeley National Laboratory, California, USA | ³Berkeley Sensor and Actuator Center, University of California Berkeley, California, USA | ⁴Kavli Energy NanoScience Institute, University of California Berkeley, California, USA | ⁵VTT Technical Research Centre of Finland Ltd, Espoo, Finland | ⁶VTT Technical Research Centre of Finland Ltd, Oulu, Finland | ⁷School of Chemical Engineering, Sungkyunkwan University, Suwon, Republic of Korea

Correspondence: Ali Javey (ajavey@berkeley.edu)

Received: 24 June 2025 | **Revised:** 10 November 2025 | **Accepted:** 25 November 2025

Keywords: disposable electronics | highly deformable microfluidic sweat sensors | roll-to-roll processing | scalable manufacturing

ABSTRACT

Disposable sweat sensors are essential tools for sweat-based diagnostics, enabling comprehensive insights into sweat physiology. To support widespread applications and large-scale studies, it is critical to develop sensors that are mass-producible, user-friendly, and capable of delivering consistent performance. Roll-to-roll processing enables scalable, and uniform manufacturing of flexible microfluidic sensors, addressing the throughput and complexity limitations of traditional methods such as photolithography and vacuum deposition. In this study, we present a highly deformable microfluidic sweat sensor fabricated via roll-to-roll processes. The sensor is constructed by laminating sweat-sensing electrodes patterned on thermoplastic polyurethane with polydimethylsiloxane microstructures to form microfluidic channels. By adapting screen printing and hot imprinting techniques for roll-to-roll manufacturing, high-throughput production is achieved. This method yields hundreds of customizable sensors per roll, exhibiting excellent mechanical flexibility, reproducible sensing performance, and scalability. Furthermore, the developed sweat sensor is demonstrated during wear on the fingertip, showcasing its capability for real-time sweat rate monitoring on an anatomically curved surface. These advancements position the roll-to-roll-fabricated sweat sensor as a promising solution for large-scale, real-time sweat diagnostic applications.

1 | Introduction

Perspiration serves as a valuable diagnostic medium for understanding internal chemical compositions and physiological responses to external stimuli [1, 2]. As chemicals in the bloodstream circulate throughout the body, they diffuse into interstitial fluid and ultimately into sweat [1]. This mechanism enables the detection of various biomarkers in sweat, albeit in dilute concentrations, including electrolytes, proteins, hormones, heavy metals, and metabolic byproducts [3–7]. Beyond chemical

analysis, the rate of sweat secretion reflects physiological and emotional states, such as thermoregulation during exercise or emotional arousal induced by stress or anxiety [1]. However, a comprehensive understanding of sweat physiology requires large-scale studies across diverse populations. To achieve this, it is critical to develop conformal, wearable sensors for user-friendly operation that are also amenable to mass production.

Traditional microfabrication techniques, including photolithography and vacuum deposition, are constrained by low through-

S.-R.K., N.D., and N.Q. contributed equally to this work.

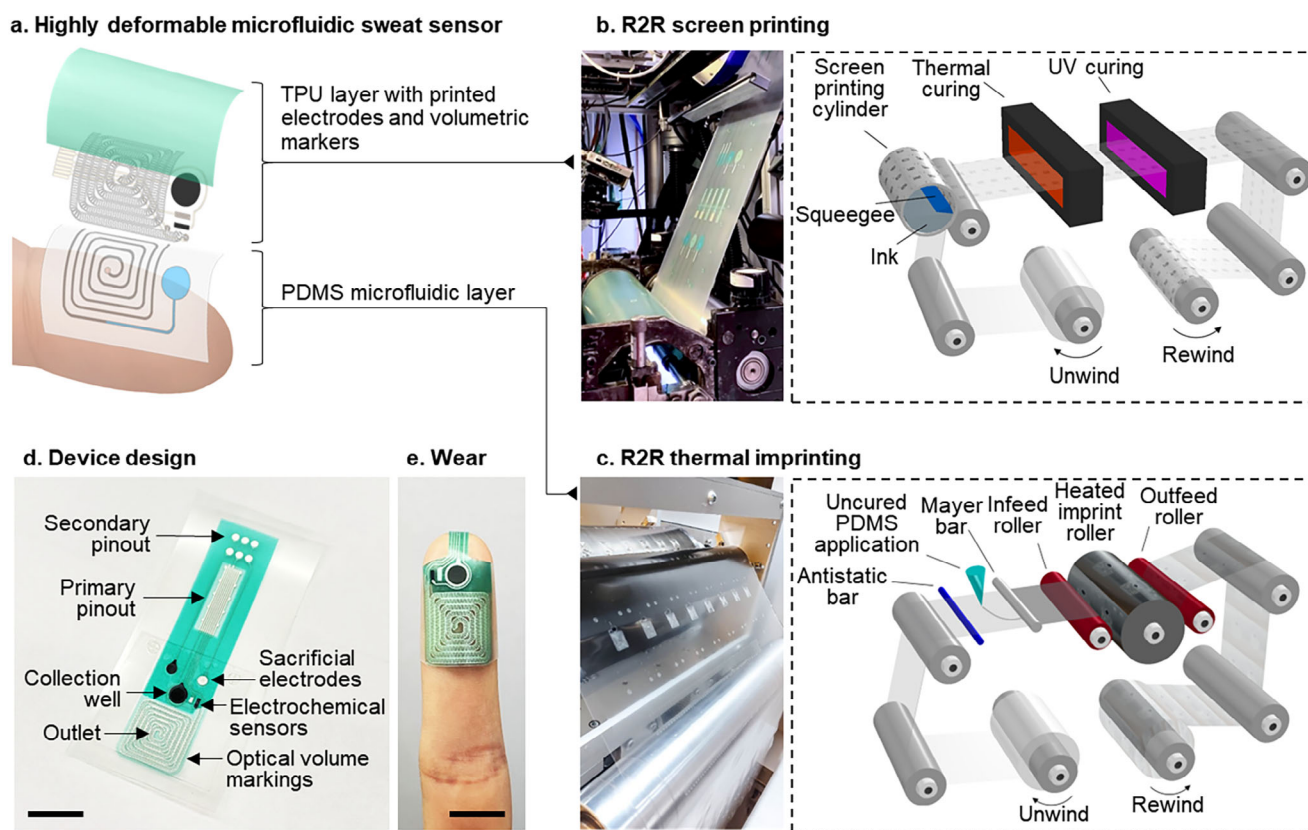


FIGURE 1 | R2R fabrication processes for highly deformable microfluidic sweat sensors. (a) Schematic illustration of a highly deformable microfluidic sweat sensor. (b) Patterned electrodes and volumetric markers are printed on TPU via R2R screen printing. (c) The microfluidic layer is fabricated on PDMS using R2R thermal imprinting. (d) Photograph of bare TPU layer showing electrodes and optical volume markings. (e) Photograph of assembled device worn on the fingertip. (Scale bars: 1 cm).

put and high complexity [8, 9]. In contrast, printed electronics, via direct additive manufacturing techniques, presents an opportunity to conserve material and energy [10, 11]. Inkjet printing is an example of an additive digital writing approach which benefits from tailorable patterning layouts using software. However, the method requires a printhead to raster across the printing area, presenting a bottleneck for high throughput manufacturing [12]. Screen printing is another additive method in which ink is transferred by a squeegee through patterned open regions of a steel or polymeric mesh screen onto the deposition area. Rotary screen printing enables roll-to-roll (R2R) production, providing high throughput large area coverage [13–15].

In this study, we present a highly deformable microfluidic sweat sensor fabricated using R2R processes, specifically designed for fingertip-mounted applications. The sensor comprises thermoplastic polyurethane (TPU) patterned with chemical sensing electrodes and volumetric markers, and an elastomeric polydimethylsiloxane (PDMS) microchannel (Figure 1a). In our prior work, we employed lithographic batch processing to fabricate PDMS microfluidics for finger mounted sweat sensors [16]. To adapt the fabrication steps for continuous roller-based manufacturing, the TPU-based layers were patterned via rotary screen printing (Figure 1b) and PDMS microstructures were directly molded using a hot imprint roller (Figure 1c). This R2R-compatible fabrication strategy enables high-throughput production, significantly improving scalability over conventional

photolithography-based methods. Each R2R-manufactured roll yields hundreds of customizable sensors that can be readily customized and integrated with diverse chemical sensing elements (Figure 1d). The highly deformable device conforms well to the curved fingertip surface, where bending strain is inevitable during attachment, enabling reliable sweat collection and sensing performance on this high-curvature skin location, as confirmed by on-body evaluations (Figure 1e).

2 | Results and Discussion

As shown in Figure 2a, each R2R-manufactured roll yields hundreds of components, the PDMS microfluidic layer and the printed TPU layer, which can be laminated to form enclosed microfluidic channels (width 400 μm , height 200 μm). To assess the deformability of the sensor platform, the bare TPU layer with printed sensing electrodes and volumetric markers was first subjected to various mechanical deformations, including 35% uniaxial strain, 2 mm radius bending, folding, 360° twisting, and localized poking (Figure 2b). The TPU layer exhibited excellent mechanical resilience, remaining structurally intact under all conditions (Figure 2b i–v). Subsequently, in Figure 2c, we evaluated the fully laminated microfluidic device. The TPU and PDMS layers were precisely aligned and bonded via (3-aminopropyl)triethoxysilane (APTES) treatments to form enclosed microfluidic channels. As an initial test, uniaxial

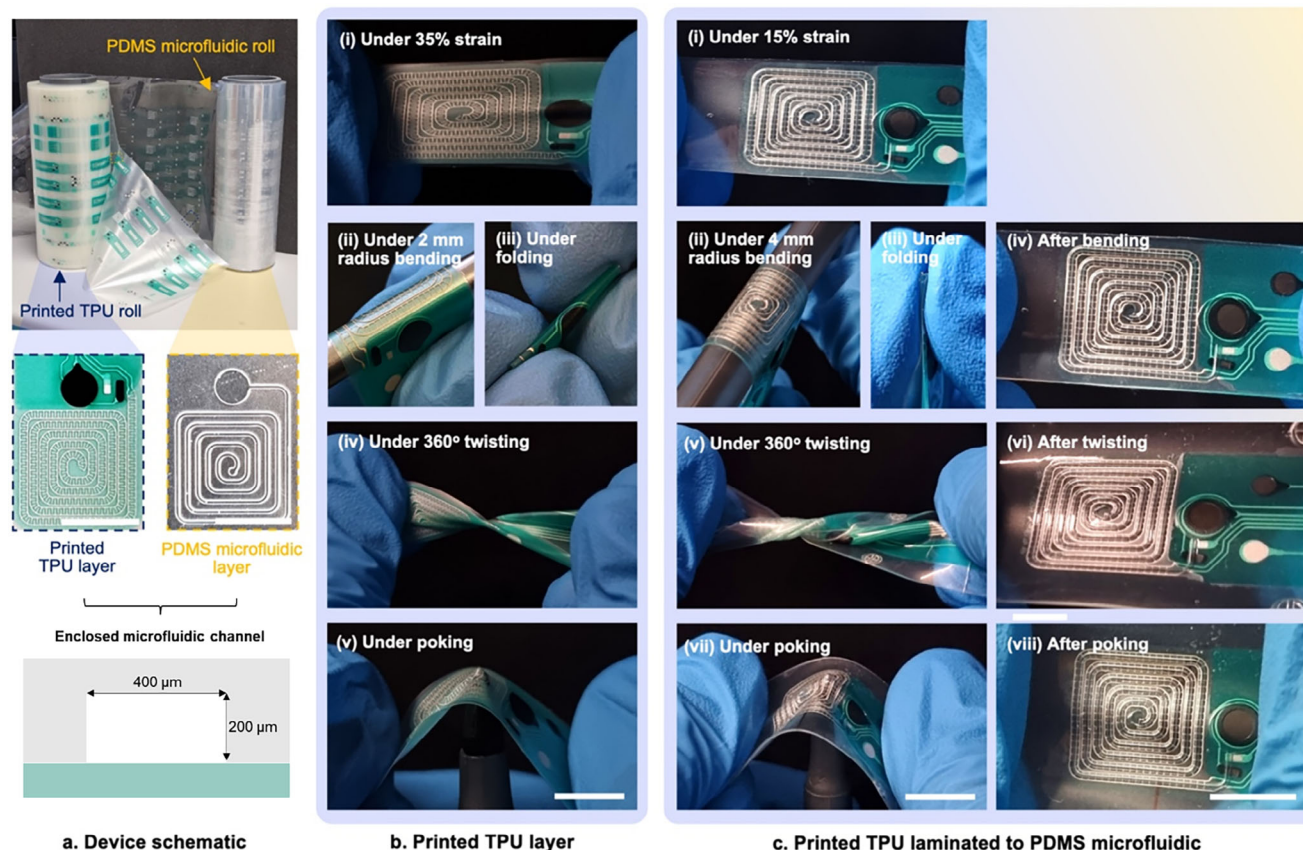


FIGURE 2 | Mechanical robustness of the TPU layer and of the fully laminated microfluidic sweat sensor. (a) Photograph of R2R-fabricated PDMS microfluidic layer and printed TPU layer rolls. Enlarged optical images show the microfluidic pattern and electrode/marker patterns. (b) Optical images of the bare TPU layer under (i) 35% strain, (ii) 2 mm radius bending, (iii) folding, (iv) 360° twisting, and (v) poking deformation. (c) Optical images of the fully integrated sensor under (i) 15% uniaxial strain, (ii) 4 mm radius bending and (iii) folding. (iv) No structural damage was observed after deformation. (v) Twisting the device 360° demonstrated high mechanical resilience, with (vi) the sensor returning to its original shape. (vii) Under poking deformation, the laminated structure remained intact. (viii) Post-deformation images confirm the structural integrity and durability of the fully laminated device under various mechanical stresses. (Scale bars: 1 cm).

stretching was applied to the integrated device (Figure 2c i). The sensor maintained its structural integrity under moderate strain (15%). Under milder deformation, such as 4 mm radius bending (Figure 2c ii) or folding (Figure 2c iii), the laminated device fully recovered without delamination. Furthermore, the sensor withstood 360° twisting (Figure 2c v) and localized poking (Figure 2c vii), which introduced biaxial strain, without structural failure. As in Figure 2c (iv, vi, viii), post-deformation images confirmed that the device returned to its original shape after all tested deformations, demonstrating the high mechanical durability and resilience of the integrated sweat sensor.

Our R2R-printed microfluidic sweat sensor has a microfluidic channel with defined inlet and outlet regions (Figure 3a). For chemical sensing, a working electrode is positioned directly beneath the inlet, enabling real-time detection of newly secreted sweat. This carbon electrode can be functionalized for chemical-specific sensing. The remaining two electrodes serve as a reference electrode (silver/silver chloride, Ag/AgCl) and counter electrode (carbon), with the latter not employed for the 2-electrode potentiometric measurements during this work, but available if a 3-electrode system were needed for future studies. Sweat flows through the microfluidic channel from the inlet to outlet. For

sweat rate sensing, linear markings are precisely aligned along the microfluidic path. As the sweat sample advances through the channel, we can track progression of the fluid front with periodic imaging for quantification of the sweat secretion rate.

To confirm the robustness of the microfluidic interface under mechanical stress, we made optical observations of the aligned device before and after stress was applied. After alignment, the microfluidic channel was filled with dyed water to enhance visualization. For the uniaxial stretching test (Figure 3b), up to 45% strain was applied to a device with full channel and no extra fluid at the inlet or outlet. Typical deformation induced by body curvature might be about 10% strain, but only at 15% strain does the channel experience much volume change, as seen by fluid beginning to draw away from the inlet and outlet, and only at 45% strain does the device rupture, illustrating the sensor's suitability for many wearable applications below this degree of strain [17]. Tuning of material thickness could be explored in future work to further improve the sensor's mechanical tolerance if needed for certain applications.

For the bending test (radius: 6.35 mm) and the twisting test (360°) shown in Figure 3c, again the channel was filled but the

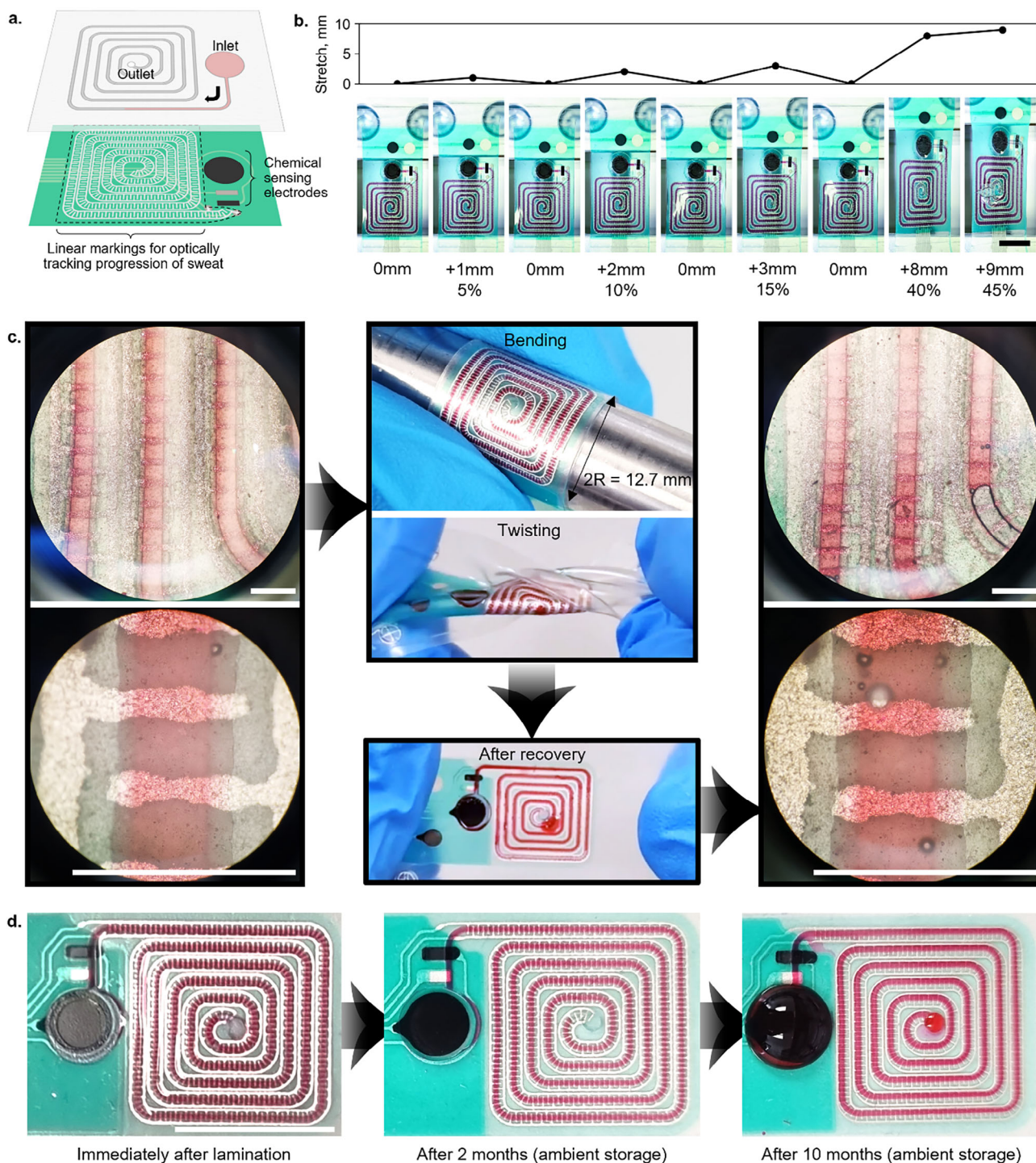


FIGURE 3 | Mechanical stability of filled microfluidic channels in the fully laminated microfluidic sweat sensors. (a) Schematic illustration of the highly deformable microfluidic sweat sensor alignment. The microfluidic channel was filled with red-dyed water during the mechanical stability tests. (b) Uniaxial stretching was performed on a stretching jig with rupture not until 45% strain. (Scale: 1 cm) (c) Optical microscope images of the microfluidic channel were compared before and after two steps of deformation including bending with a radius of 6.35 mm and twisting by 360° . (d) Optical images of the microfluidic channels from the same lamination batch taken immediately after lamination, after 2 months, and after 10 months of ambient storage, confirming long-term structural stability. (Scale bars: 1 mm).

inlet was empty prior to deformation. The bending radius of 6.35 mm was selected to approximate the curvature of the human fingertip, reflecting realistic deformation during on-skin application. Following these tests, optical microscopy revealed the presence of small air bubbles and partially unfilled regions within

the microchannel. However, the bonded structure remained grossly intact, and no critical delamination or leakage was observed. These results demonstrate that the microfluidic interface remains functionally stable under typical levels of mechanical stress expected in on-body applications. Furthermore, the

laminated microfluidic channels maintained their structural integrity after 2 and 10 months of ambient storage, confirming excellent long-term stability of the bonded TPU/PDMS assembly (Figure 3d).

To evaluate the device's applicability for wearable sweat collection and sweat rate monitoring, we conducted measurements on the fingertip using the R2R-processed, highly deformable microfluidic sweat sensor (Figure 4). To enable consistent sweat transport into the microfluidic channel, an agarose-glycerol hydrogel film was used to fill the dead volume of the inlet, as described in previous work [16]. The hydrogel prefills the inlet region and enables rapid sweat delivery to the sensing region upon secretion. Sweat progression through the channel was monitored optically (Figure 4a). A measurable signal was observed when sweat reached the first marker, ~23 min after mounting the sensor on the finger, and subsequent progression continued until ~41 min, indicating sustained thermoregulatory sweat secretion. Based on this progression, the sweat rate at the fingertip was estimated to be approximately 0.75 $\mu\text{L}/\text{min}/\text{cm}^2$ (Figure 4b). A repeated on-body measurement under the same conditions (Figure 4c,d) yielded a comparable sweat progression trend, with a sweat rate of the same order of magnitude (approximately 0.25 $\mu\text{L}/\text{min}/\text{cm}^2$), confirming reproducible sweat collection and flow rate analysis across independent trials.

To evaluate the chemical sensing performance of the flexible, R2R-processed sweat sensor, we studied the effects of mechanical strain at three levels: 1) simple relative conductance of printed interconnects and sensor pads, 2) electrochemical characteristics of printed sensor pads, and 3) signal output of functionalized sensors. First, the conductance through a pair of sensor pads (carbon and Ag/AgCl) and interconnects (Ag) was measured at three levels of uniaxial strain up to 10%. As shown in Figure 5a, the printed electrical path retains a mean of 97% relative conductance at 3.3% strain, 91% at 6.7% strain, and 84% at 10% strain.

Second, cyclic voltammetry (CV) was used to evaluate the electrochemical behavior of the printed sensing pads under strain, as shown in Figure 5b. The measurement was performed between the working and reference electrodes in potassium ferricyanide redox probe solution, using a 2-electrode configuration. This setup was selected to monitor relative changes in current response caused by mechanical deformation rather than to control the exact potential with respect to the reference electrode, thereby enabling assessment of the interfacial stability of the carbon electrodes. Even when the device was stretched up to 20% of its original length, the oxidation and reduction potentials, along with the corresponding current magnitudes, remained stable, confirming the robustness of the carbon electrode surfaces, which were designed without underlying silver to maintain a consistent electrochemical interface with the solution. Further, the small observed change is an increase in current magnitude during strain, which can be attributed to the increase in sensing pad surface area.

Finally, as illustrated in Figure 5c, we conducted potentiometric measurements of two electrolytes using ion-sensitive functional layers. Deposited on the carbon working electrodes, the functional layers are Na^+ ionophore-based selective membrane and Cl^- sensitive FeCl_3 layer, alongside an Ag/AgCl reference

electrode integrated onto the same R2R-processed substrate, configured based on our previous designs [3, 16, 18, 19]. The potentiometric responses of the Na^+ and Cl^- sensors under applied strains of 0%, 5%, and 10% are shown. To evaluate the reproducibility, two independently fabricated sensors were tested under each strain condition, and the average responses are presented. The slope for each case was obtained from linear fitting, and a total of six slope values were used for a combined linear fit. The Na^+ and Cl^- sensors exhibited near-Nernstian behavior, with mean slopes of 58.47 mV/decade ($R^2 = 0.998$) and -59.61 mV/decade ($R^2 = 0.997$), respectively. These results confirm both the reproducibility and mechanical robustness of the R2R-processed platform for strain-tolerant sweat electrolyte sensing.

3 | Conclusions

In this study, we demonstrated a highly deformable microfluidic sweat sensor produced via R2R manufacturing. The R2R-compatible screen printing and hot imprinting processes enabled high-throughput production of hundreds of sensors per roll. By laminating soft TPU and PDMS microstructures, we formed enclosed microfluidic channels that retained mechanical integrity under various deformations. The fingertip-mounted design allowed reliable sweat collection on a highly curved surface, confirming the sensor's mechanical adaptability and user comfort. This work focused on validating the scalable fabrication and on-body sensing performance of the platform, which establishes the foundation for future large-scale physiological studies using sweat analysis. These combined features make the device highly suitable for large-scale deployment in sweat-based diagnostics and continuous, real-time physiological monitoring. Overall, this work represents a significant step toward the development of accessible, skin-integrated wearable sensors that meet both performance and manufacturability requirements.

4 | Experimental Section

4.1 | Sensor Fabrication

To fabricate printed electrode structures, a roll of TPU (Covestro Plaiton U073, 100 μm thick) was R2R laminated with a polyethylene terephthalate (PET) carrier foil (DuPont Melinex ST506, 75 μm thick), and thermally pretreated (140°C oven, dwell time ~3.5 min) to assist registration by avoiding dimensional changes in the substrate during printing, before rotary screen printing with SPGPrint RotaPlate screens. Printed layers were manually registered to one another by monitoring the alignment of fiducial markings using a camera module mounted on the printing line. 7 layers were overprinted: 1) insulator (Loctite EDAG 452SS, 2 x UV cured at 50 and 80% power, 4 m/min), 2) silver (Asahi LS-411AW, 120°C oven, 2 m/min, dwell time 180 s), 3&4) carbon (Loctite EDAG PF-407A, 120°C oven, 3 m/min, dwell time 144 s), 5) Ag/AgCl (Nagase ChemteX CI-4040, 120°C oven, 2 m/min, dwell time 180 s), 6&7) insulator (Loctite EDAG 452SS, 2 x UV cured at 50 and 80% power, 4 m/min). Electrolyte sensors were fabricated on top of the R2R-processed electrodes using the methods described in our previous studies [3, 16]. The Na^+ ion sensor was prepared by drop-casting

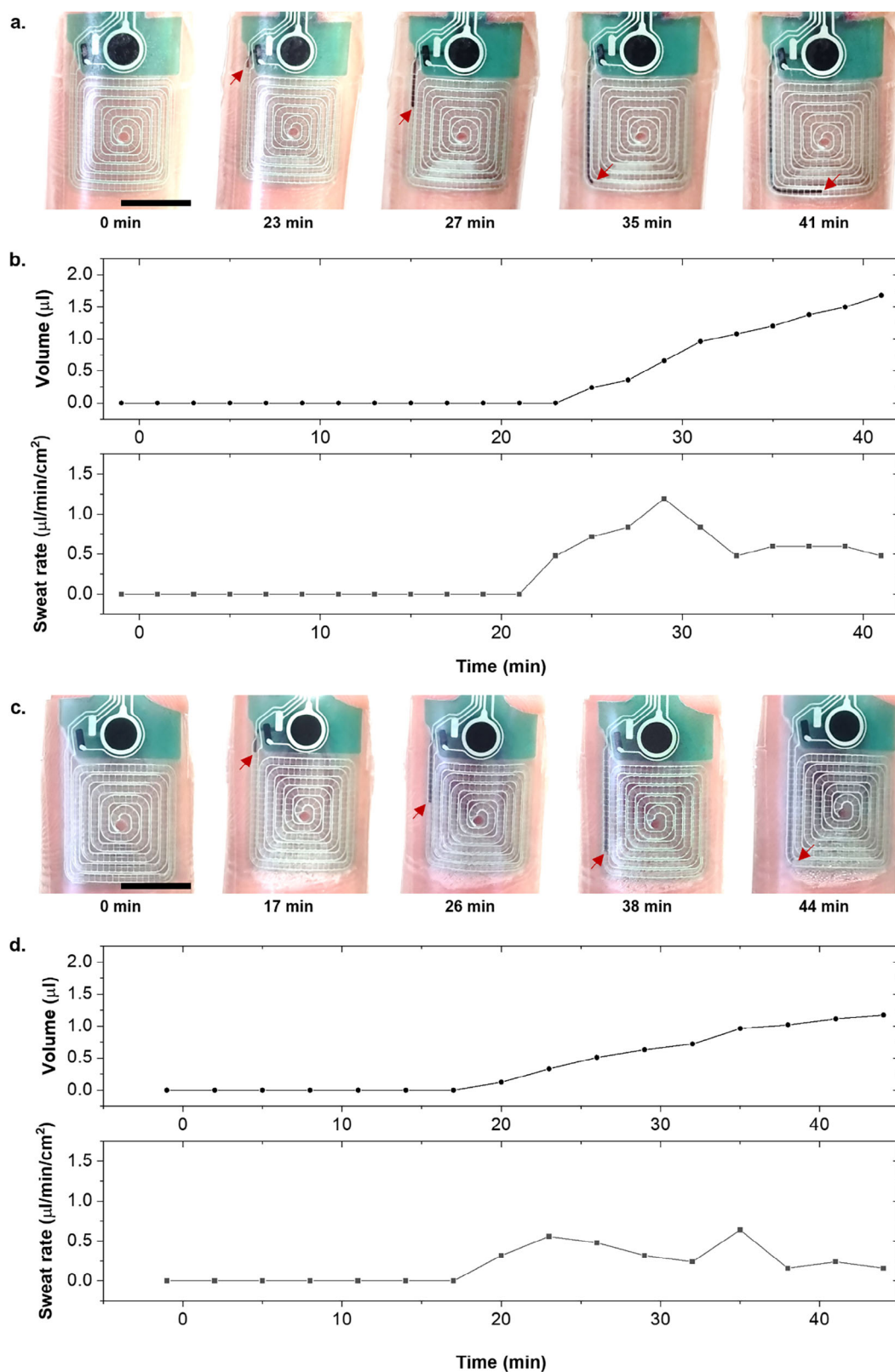


FIGURE 4 | Wearability and optical sweat rate monitoring of R2R-processed highly deformable microfluidic sweat sensors. (a) Sequential images showing the sensor conformally adhered to the curved skin surface of a finger, with red arrows indicating sweat progression through the spiral microfluidic channel. (Scale bar: 1 mm) (b) Sweat rate quantified by optical tracking of the sweat front in the microfluidic channel. (c,d) Results from an independent repeated trial under the same conditions, confirming the reproducibility of sweat collection and flow rate measurement.

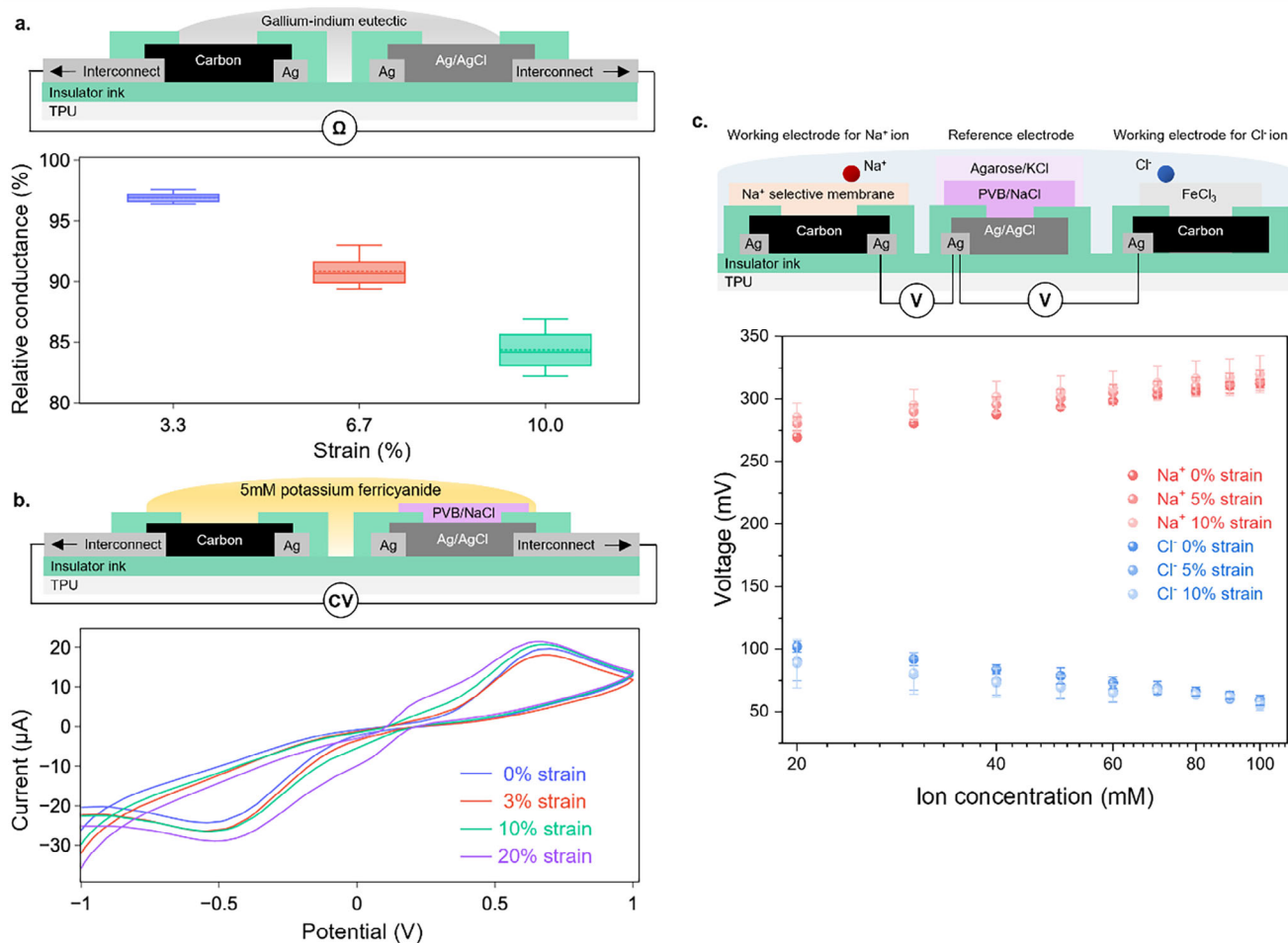


FIGURE 5 | Demonstration of electrochemical sensing capability of R2R-processed highly deformable microfluidic sweat sensors. (a) Relative conductance across chemical sensing electrodes and interconnects at 3.3%, 6.7%, and 10% strain, as measured over 10 sequential stretching cycles. The measurement was taken at the device pinout with working and reference electrodes shorted together by eutectic gallium-indium. (b) CV curves after sequential stretching to 3%, 10%, and 20% strains. The CV sweeps were done from -1 to $+1$ V at 100 mV/s with a redox probe solution connecting working and reference electrodes (70 μ L of 5 mM potassium ferricyanide in PBS 7.4). (c) Sensing layers and measurement scheme for Na^+ and Cl^- ions, functionalized on the R2R-patterned electrodes on TPU under applied strains of 0% , 5% , and 10% . All stretching speeds are 2 mm/s.

a Na^+ -selective membrane solution onto the R2R-printed carbon electrode. The Cl^- ion sensor was fabricated by treating carbon electrode with 0.1 M FeCl_3 (97%, Sigma-Aldrich, USA) in deionized water for 1 min. The reference electrode was prepared by first treating Ag/AgCl-printed electrode with 0.1 M FeCl_3 under the same conditions, followed by sequential coating with PVB/NaCl solutions.

4.2 | Microfluidic Channel Fabrication and Lamination

Microfluidic channels were R2R imprinted using processing equipment and methods described in detail in our earlier work [20]. Briefly, a steel plane shim with 200 μ m deep channels (HP Etch) was manually polished and then welded into a sleeve form (MK fluidics) that was subsequently slotted onto an embossing cylinder. The carrier substrate (PET, Melinex ST506, 125 μ m thick) was treated with atmospheric corona, then PDMS (Wacker Elastisol RT 604) was deposited by spiral bar (RK K-control coater bar,

300 μ m wet thickness) onto the running substrate (0.5 m/min) where it was impression molded with fluidic structures upon contact with the heated (135°C) embossing cylinder, resulting in 270 μ m dry thickness. Both the TPU substrate and the cured PDMS were exposed to O_2 plasma (90 W, 2 min). Following plasma treatment, the TPU substrate was coated with 1% APTES (98%, Sigma-Aldrich, USA) in deionized water and allowed to dry. The PDMS microfluidic layer was treated with 0.5% bis(2-hydroxyethyl)-APTES (62%, Gelest Inc., USA) in ethanol, rinsed, and subsequently dried with N_2 gas. The rinsed PDMS layer then underwent a second O_2 plasma treatment under the same conditions (90 W, 2 min). Finally, the treated PDMS was aligned and bonded to the activated TPU substrate to complete the assembly.

4.3 | Sensor Characterization

Controlled flow rate experiments were conducted using a Harvard Apparatus PHD 2000 Syringe Pump. Electrolyte sensor

characterizations were performed using a CHI1430 (CH Instruments, USA). The potential difference with respect to a reference electrode was measured for both sensors.

4.4 | On-Body Thermoregulatory Sweat Analysis

For thermoregulatory sweat rate sensing, an agarose-glycerol hydrogel film was used to fill the dead volume of the inlet, as described in our previous study [16]. Red food dye was incorporated into the hydrogel for clear visualization of the sweat progression. Sensors were fixed to the finger by taping over the device.

Acknowledgements

On-body human trials were carried out at the University of California, Berkeley in compliance with the human research protocol (CPHS 2014-08-6636) approved by the Berkeley Institutional Review Board (IRB). Informed consent was obtained from the subjects before enrollment in the study. This work was partially supported by Samsung Electronics Company, Ltd and Berkeley Sensors and Actuators Center (BSAC). VTT authors acknowledge the Research Council of Finland for funding research under Grant No. 351282, and the infrastructure under Grant "Printed Intelligence Infrastructure" No. 358621. Technical assistance from Jari Rekilä (technical drawings), Ulla Sarajärvi (PDMS replication), and Hannu Sääskilähti (R2R screen printing) is gratefully acknowledged. Noelle Davis acknowledges support from the National Defense Science and Engineering Graduate (NDSEG) Fellowship Program. This research was supported by the National Research Foundation (NRF) grant funded by the Korean government (MSIT) (RS-2023-00237308).

Funding

This work was partially supported by Samsung Electronics Company, Ltd and Berkeley Sensors and Actuators Center (BSAC). VTT authors acknowledge the Research Council of Finland for funding the research under Grant No. 351282, and infrastructure under grant "Printed Intelligence Infrastructure" number 358621. Noelle Davis acknowledges support from the National Defense Science and Engineering Graduate (NDSEG) Fellowship Program. This research was supported by the National Research Foundation (NRF) grant funded by the Korean government (MSIT) (RS-2023-00237308).

Conflicts of Interest

The authors declare no conflicts of interest.

Data Availability Statement

The data that support the findings of this study are available from the corresponding author upon reasonable request.

References

1. N. Davis, J. Heikenfeld, C. Milla, and A. Javey, "The Challenges and Promise of Sweat Sensing," *Nature Biotechnology* 42 (2024): 860–871, <https://doi.org/10.1038/s41587-023-02059-1>.
2. J. Zhao, H. Y. Y. Nyein, L. Hou, et al., "A Wearable Nutrition Tracker," *Advanced Materials* 33 (2021): 2006444, <https://doi.org/10.1002/adma.202006444>.
3. W. Gao, S. Emaminejad, H. Y. Y. Nyein, et al., "Fully Integrated Wearable Sensor Arrays for Multiplexed In Situ Perspiration Analysis," *Nature* 529 (2016): 509–514, <https://doi.org/10.1038/nature16521>.

4. C. Ye, M. Wang, J. Min, et al., "A Wearable Aptamer Nanobiosensor for Non-Invasive Female Hormone Monitoring," *Nature Nanotechnology* 19 (2023): 330–337, <https://doi.org/10.1038/s41565-023-01513-0>.
5. J. Ok, S. Park, Y. H. Jung, and T.-I. Kim, "Wearable and Implantable Cortisol-Sensing Electronics for Stress Monitoring," *Advanced Materials* 36 (2024): 2211595, <https://doi.org/10.1002/adma.202211595>.
6. W. Gao, H. Y. Y. Nyein, Z. Shahpar, et al., "Wearable Microsensor Array for Multiplexed Heavy Metal Monitoring of Body Fluids," *ACS Sensors* 1 (2016): 866–874, <https://doi.org/10.1021/acssensors.6b00287>.
7. A. J. Bandodkar, W. J. Jeang, R. Ghaffari, and J. A. Rogers, "Wearable Sensors for Biochemical Sweat Analysis," *Annual Review of Analytical Chemistry* 12 (2019): 1–22, <https://doi.org/10.1146/annurev-anchem-061318-114910>.
8. L. Yin, M. Cao, K. N. Kim, et al., "A Stretchable Epidermal Sweat Sensing Platform with an Integrated Printed Battery and Electrochromic Display," *Nature Electronics* 5 (2022) 694–705, <https://doi.org/10.1038/s41928-022-00843-6>.
9. S. Ma, Z. Wan, C. Wang, et al., "Ultra-Sensitive and Stable Multiplexed Biosensors Array in Fully Printed and Integrated Platforms for Reliable Perspiration Analysis," *Advanced Materials* 36 (2024): 2311106, <https://doi.org/10.1002/adma.202311106>.
10. E. Kunnari, J. Valkama, M. Keskinen, and P. Mansikkamäki, "Environmental Evaluation of New Technology: Printed Electronics Case Study," *Journal of Cleaner Production* 17 (2009) 791–799, <https://doi.org/10.1016/j.jclepro.2008.11.020>.
11. V. Pecunia, L. Petti, J. B. Andrews, et al., "Roadmap on Printable Electronic Materials for Next-Generation Sensors," *Nano Futures* 8 (2024): 032001, <https://doi.org/10.1088/2399-1984/ad36ff>.
12. B. Derby, "Inkjet Printing of Functional and Structural Materials: Fluid Property Requirements, Feature Stability, and Resolution," *Annual Review of Materials Research* 40 (2010): 395–414, <https://doi.org/10.1146/annurev-matsci-070909-104502>.
13. H. Y. Y. Nyein, M. Bariya, L. Kivimäki, et al., "Regional and Correlative Sweat Analysis Using High-Throughput Microfluidic Sensing Patches Toward Decoding Sweat," *Science Advances* 5 (2019): aaw9906, <https://doi.org/10.1126/sciadv.aaw9906>.
14. M. Bariya, Z. Shahpar, H. Park, et al., "Roll-to-Roll Gravure Printed Electrochemical Sensors for Wearable and Medical Devices," *ACS Nano* 12 (2018): 6978–6987, <https://doi.org/10.1021/acsnano.8b02505>.
15. M. Välimäki, T. Happonen, T. Karhu, et al., "Rotary-Screen Printing with Improved Registration and Dimensional Stability for Flexible Electronics," *Flexible and Printed Electronics* 10 (2025) 015003, <https://doi.org/10.1088/2058-8585/ad9d56>.
16. H. Y. Y. Nyein, M. Bariya, B. Tran, et al., "A Wearable Patch for Continuous Analysis of Thermoregulatory Sweat at Rest," *Nature Communications* 12 (2021): 1823, <https://doi.org/10.1038/s41467-021-22109-z>.
17. D.-H. Kim, N. Lu, R. Ma, et al., "Epidermal Electronics," *Science* 333 (2011): 838–843, <https://doi.org/10.1126/science.1206157>.
18. M. Dautta, L. F. Ayala-Cardona, N. Davis, et al., "Tape-Free, Digital Wearable Band for Exercise Sweat Rate Monitoring," *Advanced Materials Technologies* 8 (2023): 2201187, <https://doi.org/10.1002/admt.202201187>.
19. M. Bariya, N. Davis, L. Gillan et al., "Resettable Microfluidics for Broad-Range and Prolonged Sweat Rate Sensing," *ACS Sensors* 7 (2022): 1156–1164, <https://doi.org/10.1021/acssensors.2c00177>.
20. O. H. Huttunen, J. Hiitola-Keinänen, J. Petäjä, E. Hietala, H. Lindström, and J. Hiltunen, "Roll to Roll Imprinting PDMS Microstructures Under Reduced Ambient Pressures," *Journal of Microelectromechanical Systems* 33 (2024): 95–101, <https://doi.org/10.1109/JMEMS.2023.3336740>.